2

Dark matter and leptogenesis in the minimal scotogenic model

In this chapter, we study the minimal scotogenic model constituting an additional inert Higgs doublet and three sets of right-handed neutrinos. The scotogenic model connects dark matter, baryon asymmetry of the Universe and neutrino oscillation data. In our work, we obtain baryogenesis by the decay of TeV scale heavy neutral singlet fermion (N_2). We primarily focus on the intermediate-mass region of dark matter within $M_W < M_{DM} \leq 550$ GeV, where observed relic density is suppressed due to co-annihilation processes. We consider thermal as well as the non-thermal approach of dark matter production and explore the possibility of the lightest stable candidate being a dark matter candidate. Within the inert Higgs doublet (IHD) desert, we explore a new allowed region of dark matter masses for the non-thermal generation of dark matter with a mass splitting of 10 GeV among the inert scalars. We also see the

variation of relic abundance for unequal mass splitting among the scalars. The KamLand-Zen bound on the effective mass of the active neutrinos is also verified in this study.

2.1 Introduction

Our work is carried out depending on the idea of low mass RHN as mentioned in[68], the study of thermal leptogenesis in Ernest Ma's scotogenic model[13, 14], which is considered to be the simplest model of radiative neutrino masses. Hence, we choose the scale of the RHN in such a fashion that it can satisfy the observed value of BAU and does not bother the dark matter phenomenology. This work primarily focuses on the IHDM desert, i.e., $M_W < M_{DM} \leq 550$ GeV, wherein the generation of the relic abundance is prohibited as mentioned in various literatures[13, 33, 199]. The core reason behind this discrepancy is that in the IHDM desert, the annihilation cross-section of the dark matter is large compared to the amount necessary to produce the correct relic abundance via the freeze-out mechanism. Thus, we get an underabundant DM in this regime due to the large annihilation rates. Though the lower bound of the IHDM desert is rigid, the upper bound can be a little flexible depending on the choice of parameters such as the DM-Higgs coupling and the mass splitting between the inert scalars. Thus, we try to see the viability of IHDM desert, concentrating on the upper bound satisfying the relic abundance value with latest restrictions from direct detection experiment XENON1T[95]. The production of a correct relic in this regime can be possible by fine-tuning of the DM-Higgs coupling and suitable mass splitting of the other inert scalars.

Motivated by these factors, in this model, the SM is extended by a Higgs doublet field (η) and three singlet neutral fermions (N_k), which are odd under Z_2 symmetry, in contradiction to the SM particles which are Z_2 even. The possibility of a DM candidate comes from the Z_2 odd lightest particle. Whereas, leptogenesis is a result of the Z_2 odd fermions, i.e., the heavy RHN, which occurs via the out-of-equilibrium decay into the SM leptons and the inert Higgs doublet[33]. The entire work is carried out keeping the dark matter mass in the intermediate

dark matter mass range, also known as IHDM desert, which lies between $M_W < M_{DM} \leq 550$ GeV. Leptogenesis is obtained for this very range of dark matter mass with the decay of N_2 which is the next to lightest RHN. Also, an important criterion that is kept intact is the sum of neutrino masses and its effective mass being consistent with the constraints from Planck data and neutrinoless double beta decay experiment, KamLAND-Zen. We also check the relic abundance of the dark matter candidate (lightest of η) for different choices of mass splitting between the scalars of the inert scalar doublet. We further investigate the parameter space, i.e. the values of DM-Higgs coupling and dark matter mass for which it satisfies the bounds from relic abundance and direct detection experiment. Furthermore, we also study the mixture of thermal and non-thermal production of DM abundance for various masses within the IHDM desert. In one of the cases, we have considered mass splitting of the scalars in the inert doublet to be 10 GeV and studied the criteria that satisfy the observed relic for higher DM masses within the IHDM desert via purely thermal production as well as non-thermal production. The non-thermal production process is solely to enhance the relic of DM which is under-abundant in the IHDM desert, produced via thermal mechanism. This can be made possible by the late decay of the RHN, N_1 into DM and SM leptons for very small decay width of N_1, which further makes it incompetent to produce the BAU.

The rest of the paper is divided into five sections, where section(2.2) includes a brief introduction of the scotogenic model involving the generation of neutrino mass. In section(2.3), we discuss about the various bounds on this model. The phenomena carried out in this framework namely BAU, DM and $0\nu\beta\beta$ are included in section(2.4). A detailed numerical analysis, along with results, are shown in section(2.5) followed by the summary given in section(2.6).

2.2 Scotogenic model

Scotogenic model is an extension of the IHDM[33] and the IHDM is nothing but a minimal extension of the SM by a Higgs field which is a doublet under $SU(2)_L$ gauge symmetry with hypercharge $Y = 1$ and a built-in discrete Z_2 symmetry[33, 199, 200, 73, 72, 201–205, 34, 206, 75, 207, 36]. The necessity of this modification took place as the IHDM could only accommodate dark matter, whereas it failed in explaining the origin of neutrino masses at a renormalizable level[34]. In this model, three neutral singlet fermions N_i with $i = 1,2,3$ are added in order to generate neutrino masses and assign them with a discrete Z_2 symmetry. In view of N_i, the neutrinos can get masses in two ways. One of the ways is similar to the type-I seesaw mechanism[7, 81, 83, 84], where the neutrino masses arise as a result of N_i being Z_2 even. Also, it is limited to show no dark matter phenomenology of the IHDM and keeps the neutrino masses decoupled from the DM characteristics. Therefore, we opt for the other way in which N_i is odd under Z_2 symmetry, whereas the SM fields remain Z_2 even. Symbolic transformation of the particles under Z_2 symmetry is given by,

$$N_i \longrightarrow -N_i,\ \eta \longrightarrow -\eta,\ \Phi \longrightarrow \Phi,\ \Psi \longrightarrow \Psi, \tag{2.1}$$

where η is the inert Higgs doublet, Φ is the SM Higgs doublet and Ψ denotes the SM fermions. The new leptonic and scalar particle content can thereafter be represented as follows under the group of symmetries $SU(2) \times U(1)_Y \times Z_2$:

$$\begin{pmatrix} \nu_\alpha \\ l_\alpha \end{pmatrix}_L \sim (2, -\frac{1}{2}, +),\ l^c_\alpha \sim (1,1,+),\ \begin{pmatrix} \Phi^+ \\ \Phi^0 \end{pmatrix} \sim (2, \frac{1}{2}, +),$$

$$N_i \sim (1,1,-),\ \begin{pmatrix} \eta^+ \\ \eta^0 \end{pmatrix} \sim (2, 1/2, -). \tag{2.2}$$

The scalar doublets are written as follows :

$$\eta = \begin{pmatrix} \eta^{\pm} \\ \frac{1}{\sqrt{2}}(\eta_R^0 + i\eta_I^0) \end{pmatrix}, \quad \Phi = \begin{pmatrix} \Phi^{+} \\ \frac{1}{\sqrt{2}}(h + i\xi) \end{pmatrix}. \tag{2.3}$$

We have no Dirac mass term with ν and N; however, the similar Yukawa-like coupling involving η is allowed. Nevertheless, the scalar cannot get a VEV. The neutrino mass can be generated through a one-loop mechanism, which is based on the exchange of η particle and a heavy neutrino. In fig (1.1), we see two Higgs fields ϕ^0 are involved. They will not propagate but will acquire VEV after the EWSB.

The lagrangian involving the newly added field is :

$$\mathcal{L} \supset \frac{1}{2}(M_N)_{ij} N_i N_j + Y_{ij} \bar{L}_i \tilde{\eta} N_j + h.c \tag{2.4}$$

where, the 1^{st} term is the Majorana mass term for the neutrino singlet and the 2^{nd} term is the Yukawa interactions of the lepton. The new potential on addition of the new inert scalar doublet is:

$$\begin{aligned} V_{Scalar} =& m_1^2 \Phi^+\Phi + m_2^2 \eta^+\eta + \frac{1}{2}\lambda_1(\Phi^+\Phi)^2 + \frac{1}{2}\lambda_2(\eta^+\eta)^2 + \lambda_3(\Phi^+\Phi)(\eta^+\eta) \\ &+ \lambda_4(\Phi^+\eta)(\eta^+\Phi) + \big[\frac{\lambda_5}{2}(\Phi^+\eta)^2 + h.c.\big] \end{aligned} \tag{2.5}$$

All the parameters in eq. (2.5) are real by hermicity of the Lagrangian, except for λ_5. Since, the bilinear term $(\Phi^+\eta)$ is forbidden by the exact Z_2 symmetry, therefore one can always choose λ_5 real by rotating the relative phase between Φ and η. Furthermore, after the spontaneous symmetry breaking like in the SM, we are left with one physical Higgs boson h which resembles the SM Higgs boson, as well as four dark scalars: one CP even(η_R^0), one CP

odd(η_I^0) and a pair of charged ones ($\eta^\pm$). The masses of these physical scalars are:

$$\begin{aligned} m_h^2 &= -m_1^2 = 2\lambda_1 v^2, \\ m_{\eta^\pm}^2 &= m_2^2 + \frac{1}{2}\lambda_3 v^2, \\ m_{\eta_R^0}^2 &= m_2^2 + \frac{1}{2}(\lambda_3+\lambda_4+\lambda_5)v^2, \\ m_{\eta_I^0}^2 &= m_2^2 + \frac{1}{2}(\lambda_3+\lambda_4-\lambda_5)v^2. \end{aligned} \tag{2.6}$$

It is clear from the above equations that all the scalar couplings are written in terms of physical scalar masses and m_2 , thereby providing six independent parameters of the model to be : $\{m_2, m_h, m_{\eta_R^0}, m_{\eta_I^0}, m_{\eta^\pm}, \lambda_2\}$. Here, m_h is the mass of SM-Higgs, $m_{\eta_R^0}$, $m_{\eta_I^0}$ and $m_{\eta^\pm}$ are the masses of CP-even, CP-odd and charged scalars of the inert doublet respectively. In this work, as we have considered the CP-even scalar to be the lightest particle and a probable DM candidate, so we consider $\lambda_5 < 0$ without any loss of generality. Moreover, the mass difference between the real and imaginary component of the inert doublet η from (2.6) can be written as , $m_{\eta_R^0}^2 - m_{\eta_I^0}^2 = \lambda_5 v^2$. Therefore, in the limit $\lambda_5 \to 0$ leads to the mass degeneracy of the neutral components of the inert doublet. Again, the case of vanishing λ_5 would lead to vanishing neutrino mass, as the λ_5 in (2.5) associate with the lepton number violation term in (2.4). Therefore, considering $\lambda_5 \to 0$ allows us to recover the lepton number global symmetry, and following the 't Hooft scenario[208], the smallness of λ_5 is essential to obtain the lepton asymmetry, which would have been lost if considered to be zero, is acceptably natural. Throughout our analysis, for the coupling constants we follow the inequality relation $\lambda_4 >> \lambda_5$. We have a simplified diagram that can be split further into two diagrams and from which the mass can be easily calculated by considering mechanism after EWSB. Calculation on the basis of one diagram is sufficient and considered as other would be same except for η_R^0 replaced by η_I^0. The neutrino mass matrix arising from the radiative mass model is given

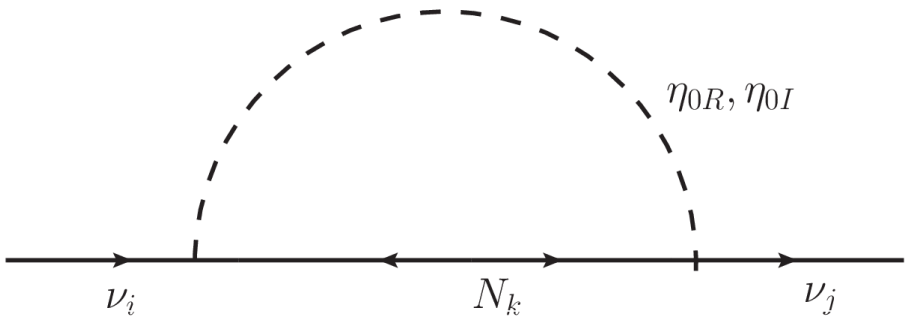

Fig. 2.1 One-loop diagram with exchange of η_R^0 and η_I^0. ν_i and ν_j representing two different generations of active neutrinos. N_k is the right handed neutrino.

by[201, 209]:

$$\begin{aligned} M_{ij}^{\nu} &= \sum_k \frac{h_{ik}h_{jk}}{16\pi^2} M_k \left[\frac{m^2_{\eta_R^0}}{m^2_{\eta_R^0} - M_k^2} ln \frac{m^2_{\eta_R^0}}{M_k^2} - \frac{m^2_{\eta_I^0}}{m^2_{\eta_I^0} - M_k^2} ln \frac{m^2_{\eta_I^0}}{M_k^2} \right] \\ &\equiv \sum_k \frac{h_{ik}h_{jk}}{16\pi^2} M_k [L_k(m^2_{\eta_R^0}) - L_k(m^2_{\eta_I^0})], \end{aligned} \tag{2.7}$$

where M_k represents the mass eigenvalue of the mass eigenstate N_k of the neutral singlet fermion N_k in the internal line with indices j=1,2,3 running over the three neutrino generation with three copies of N_k. The function $L_k(m^2)$ used in eq. (2.7) is given by:

$$L_k(m^2) = \frac{m^2}{m^2 - M_k^2} \ln \frac{m^2}{M_k^2} \tag{2.8}$$

In our study, we calculate the Yukawa couplings by the incorporation of the constraints on the sum of neutrino masses[210] and the neutrino oscillation data[66]. For simplicity of the Yukawa coupling calculation, we write the mass formula given by eq. (2.7), in the form similar to type-I seesaw formula[211]:

$$M_\nu = Y \Lambda^{-1} Y^T, \tag{2.9}$$

where Λ is a diagonal matrix represented by[212]:

$$\Lambda_k = \frac{M_k}{16\pi^2}\left[\frac{m^2_{\eta^0_R}}{m^2_{\eta^0_R}-M_k^2}\,ln\frac{m^2_{\eta^0_R}}{M_k^2} - \frac{m^2_{\eta^0_I}}{m^2_{\eta^0_I}-M_k^2}\,ln\frac{m^2_{\eta^0_I}}{M_k^2}\right]. \tag{2.10}$$

The light neutrino mass matrix (2.7) can be diagonalised by an unitary matrix known as the *Pontecorvo-Maki-Nakagawa-Sakata(PMNS)* matrix.

The diagonal light neutrino mass matrix can be written as:

$$M_\nu^{diag} = U^\dagger M_\nu U^* \tag{2.11}$$

Also, we use a special yet one of the most popular types of parametrization known as the *Casas-Ibarra parametrization* [213] in order to link the Yukawa coupling with the light neutrino parameters.

$$Y = U\sqrt{M_\nu^{diag}}R^\dagger\sqrt{\Lambda}, \tag{2.12}$$

where R is a complex orthogonal matrix satisfying the condition $R^TR = 1$. We also parameterized the R matrix as per our convenience and the orthogonal complex matrix R takes the form,

$$R = \begin{pmatrix} 0 & \cos Z & \sin Z \\ 0 & -\sin Z & \cos Z \\ 1 & 0 & 0 \end{pmatrix}, \tag{2.13}$$

where, $Z = (z_R + iz_I)$ with $z_R, z_I \in [0, 2\pi]$[214]. In our case, we consider the values 1.42 and 1.6232 respectively for normal hierarchy(NH). In the case of inverted hierarchy, we arbitrarily choose lower values of z_R= 0.22 and z_I= 0.58, which contributes to a slight difference in the baryogenesis plot as a function of RHN N_2. This choice of the orthogonal matrix R is made to calculate the Yukawa couplings related by the *Casas- Ibarra parametrization* given in eq.(2.12), in order to obtain a non-zero complex term for $(Y^\dagger Y)_{22}$ which is inversely proportional to the CP asymmetry ε_2. Since ε_2 is directly dependent on $(Y^\dagger Y)_{21}$ and $(Y^\dagger Y)_{23}$ as well, the requirement of these quantities to be non-zero is a must. Therefore, such a choice

of R as in eq.(2.13) is adequate in fulfilling the foresaid criteria. The evaluated Yukawa matrix in NH mode from (2.12) is given by,

$$Y_{NH} = \begin{pmatrix} -9.27224\times10^{-6}+0.0000412i & -0.0013963-0.00034838i & -0.0443544 \\ -0.00001429+0.00004271i & -0.0014436-0.0005405i & -0.022009+0.004795i \\ 5.60918\times10^{-6}-0.00004588i & 0.001558+0.000227i & 0.020248+0.00483i \end{pmatrix} \tag{2.14}$$

and that for IH mode is given by:

$$Y_{IH} = \begin{pmatrix} -0.00002917+3.70529\times10^{-6}i & 0.00010793+0.00024547i & 0.0743562 \\ -0.000025069+6.74852\times10^{-6}i & 0.000070818+0.00021745i & -0.0409688+0.0062949i \\ 0.000031937-6.25485\times10^{-6}i & -0.00013739-0.0002630i & 0.0367029+0.0055138i \end{pmatrix} \tag{2.15}$$

Also, for the Yukawa coupling values obtained in this work, the lepton flavor violating process $l_\alpha \to l_\beta \gamma$ is possible. Bounds from various LFV processes in this model are discussed in the following subsection.

2.3 Bounds on this model

2.3.1 Lepton flavor violating processes

It is well known that lepton flavor violating processes put significant bound on the model parameter space. The size of the LFV is controlled by the lepton number violating Yukawa couplings Y_{ij}. The LFV processes such as $l_\alpha \to l_\beta\gamma$, $l_\alpha \to 3l_\beta$ and $\mu - e$ conversion in nuclei within the framework of scotogenic model put significant bounds[212].

In case of radiative lepton decay, the branching ratio of $l_\alpha \to l_\beta\gamma$ is given by-

$$\mathrm{Br}(l_\alpha \to l_\beta\gamma) = \frac{3(4\pi^3)\alpha_{em}}{4G_F^2}|A_D|^2\mathrm{Br}(l_\alpha \to l_\beta \nu_\alpha \bar{\nu\beta}) \tag{2.16}$$

For three body decay process like $l_\alpha \to 3l_\beta$, the branching ratio is given by-

$$\begin{aligned}\mathrm{Br}(l_\alpha \to 3l_\beta) =& \frac{3(4\pi^2)\alpha_{em}^2}{8G_F^2}\left[|A_{ND}|^2 + |A_D|^2\left(\frac{16}{3}\log\left(\frac{m_\alpha}{m_\beta}\right) - \frac{22}{3}\right)\right. \\ &\left. + \frac{1}{6}|B|^2 + \left(-2A_{ND}A_D^* + \frac{1}{3}A_{ND}B^* - \frac{2}{3}A_DB^* + h.c\right)\right] \\ &\times \mathrm{Br}(l_\alpha \to l_\beta \nu_\alpha \bar{\nu\beta})\end{aligned} \tag{2.17}$$

The conversion rate, normalized to the the muon capture rate, can be expressed as -

$$\begin{aligned}\mathrm{CR}(\mu - e, Nucleus) =& \frac{p_e E_e m_\mu^3 G_F^2 \alpha_{em}^3 Z_{eff}^4 F_p^2}{8\pi^2 Z\Gamma_{capt}} \times \left[|(Z+N)(g_{LV}^{(0)} + g_{LS}^{(0)}) + \right. \\ &(Z-N)(g_{LV}^{(1)} + g_{LS}^{(1)})|^2 + |(Z+N)(g_{RV}^{(0)} + g_{RS}^{(0)}) + \\ &\left.(Z-N)(g_{RV}^{(1)} + g_{RS}^{(1)})|^2\right]\end{aligned} \tag{2.18}$$

The notations we have used in the above mentioned relations are explicitly taken from[212]. The MEG collaboration has been able to set the impressive bound on muon decay $\mathrm{Br}(l_\alpha \to l_\beta\gamma) < 4.2 \times 10^{-13}$[215]. In case of $l_\alpha \to 3l_\beta$ decay contraints comes from SINDRUM experiment to be $\mathrm{Br}(l_\alpha \to 3l_\beta) < 10^{-12}$ which has been set long ago. In our analysis, for NH, we obtain: $\mathrm{Br}(\mu \to e\gamma) = 6.22 \times 10^{-18}$, $\mathrm{Br}(\mu \to 3e) = 7.31839 \times 10^{-34}$, $\mathrm{CR}(\mu \to e) = 2.64278 \times 10^{-36}$. Similarly for IH, we obtain: $\mathrm{Br}(\mu \to e\gamma) = 8.36708 \times 10^{-19}$, $\mathrm{Br}(\mu \to 3e) = 3.60477 \times 10^{-34}$, $\mathrm{CR}(\mu \to e) = 9.59989 \times 10^{-37}$. For Yukawa coupling values less than 10^{-4}, as required by neutrino mass constraints, one can get branching ratio value for the process $l_\alpha \to l_\beta\gamma$ below the experimental bound given by MEG collaboration[216]. However, we have not considered LFV processes related to τ lepton (such as $\tau \to e\gamma,\ \tau \to \mu\gamma,\ \tau \to 3e,\ \tau \to 3\mu$) in our study, as they are less sensitive to experiments (exceptions in case of high-luminosity electron-positron collider experiments like SuperB, Belle II may improve the bound, which we have not considered in our study). Hence, they do not have robust bounds on our model parameter spaces.

2.3.2 Stability constraints

The stability of the scalar potential demands that the potential should be bounded from below, *i.e.*, it should not approach negative infinity along any direction of the field space at large field values. With large field the quadratic terms of the scalar potential in eq.(2.5) are smaller compared to the quartic terms. This scalar potential will be bounded from below if the following conditions are satisfied[200],

$$\lambda_1(\Lambda) \geq 0; \quad \lambda_2(\Lambda) \geq 0; \quad \lambda_3(\Lambda) \geq -2\sqrt{\lambda_1(\Lambda)\lambda_2(\Lambda)} \text{ and } \lambda_{L,S}(\Lambda) \geq -\sqrt{\lambda_1(\Lambda)\lambda_2(\Lambda)}.$$

Here, $\lambda_{L,S} = \frac{1}{2}(\lambda_3 + \lambda_4 \pm \lambda_5)$. The coupling constants are evaluated at a scale Λ using RG equations.

2.3.3 Perturbativity constraints

For IDM to behave as a perturbative quantum field theory at a given scale Λ, one must impose the condition on the couplings of the potential (2.5), and they are as follows[217],

$$|\lambda_1(\Lambda),\ \lambda_2(\Lambda),\ \lambda_3(\Lambda),\ \lambda_4(\Lambda),\ \lambda_5(\Lambda)| \leq 4\pi. \tag{2.19}$$

2.3.4 Unitarity bounds

Unitarity bounds on the couplings are evaluated by considering scalar-scalar, gauge boson-gauge boson, and scalar-gauge boson scatterings[217]. In general, unitarity bounds are the couplings of the physical bases of the scalar potential. Nevertheless, the couplings for the scalars are quite complicated, therefore we consider the couplings of the non-physical bases before EWSB. Then the S-matrix, which is expressed in terms of the non-physical fields, is transformed into an S-matrix for the physical fields by making a unitary transformation[218–220]. The unitarity of the S-matrix demands the absolute eigenvalues of the scattering matrix should be less than 8π up to a particular scale. In our potential, bounds come from the

eigenvalues of the corresponding S-matrix are as follows,

$$
\begin{aligned}
&|\lambda_3 \pm \lambda_4| \leq 8\pi, \quad |\lambda_3 \pm \lambda_5| \leq 8\pi, \\
&|\lambda_3 + 2\lambda_4 \pm 3\lambda_5| \leq 8\pi, \\
&\left|\lambda_1 + \lambda_2 \pm \sqrt{(\lambda_1 - \lambda_2)^2 + \lambda_4}\right| \leq 8\pi, \\
&\left|3\lambda_1 + 3\lambda_2 \pm \sqrt{9(\lambda_1 - \lambda_2)^2 + (2\lambda_3 + \lambda_4)^2}\right| \leq 8\pi, \\
&\left|\lambda_1 + \lambda_2 \pm \sqrt{(\lambda_1 - \lambda_2)^2 + \lambda_5}\right| \leq 8\pi.
\end{aligned}
\tag{2.20}
$$

2.4 Phenomenology in scotogenic framework

2.4.1 Baryogenesis via leptogenesis

A fascinating way to dynamically produce the observed baryon asymmetry of the Universe (BAU) is via the mechanism of leptogenesis[67]. There arises an intrinsic limitation of the standard thermal leptogenesis, which is due to the requirement of a very high right-handed neutrino (RHN) mass scale. In the most generic scenario, occasionally known as the vanilla leptogenesis, there exists an absolute lower bound on the mass of the lightest RHN to be $M_1 \simeq 10^9$ GeV[86, 221]. Whereas, in the case of the scotogenic model, with three Z_2 odd SM singlet fermions, one can bring down the limit on the lightest RHN mass scale to be as low as 10 TeV[68, 35]. In our work, we have taken the lightest RHN mass scale of the range $10^4 - 5 \times 10^5$ GeV, and that of the heavier RHNs, N_2 and N_3 of the range $10^7 - 5 \times 10^8$ GeV and $10^{12} - 5 \times 10^{13}$ GeV respectively for generating the required baryogenesis. Since it is kinematically allowed via the Yukawa interactions, the SM singlet neutral fermions decay into the SM leptons, and the inert Higgs doublet η. In our work, we have considered the non-thermal production of DM within the IHDM desert via late decays of N_1 and thereby a small decay width of N_1 is considered for it to decay after DM freezes-out. Again, due to the consideration of the IHDM desert, the freeze-out will occur below the sphaleron temperature. Thus, the lifetime of N_1 will be more than sphaleron time prohibiting its decay to lepton

asymmetry in to the observed baryon asymmetry above the sphaleron scale. Hence, lepton asymmetry is generated only because of the asymmetry created by the decay of N_2, which is the next to lightest RHN. The asymmetry produced by N_3 decays is considered negligible as a result of strong washout effect mediated by N_2 or N_3 itself. This leptogenesis is further converted into the baryon asymmetry of the Universe (BAU) by the electro-weak sphaleron phase transition[222]. The simultaneous Boltzmann equations for N_2 decay and formation of N_{B-L} are to be solved to obtain the results for baryogenesis. The B-L calculation is mainly governed on the comparison between the Hubble parameter and the decay rates for $N_2 \to l\eta, \bar{l}\eta^*$ processes, which will have a certain impact on the asymmetry as well as on the CP-asymmetry parameter ε_2. We now further look into the various expressions and quantities that are required for the calculation of thermal leptogenesis in the scotogenic model. As essential in thermal leptogenesis, we need to distinguish between a weak washout and a strong washout regime. The differentiation is characterized based on the values of the decay parameter, K_2, which can be expressed as given in eq.(1.52).

Leptogenesis occurs above the electroweak scale during the era of radiation domination. The Hubble parameter can therefore be expressed in terms of T as follows:

$$H = \sqrt{\frac{8\pi^3 g_*}{90}} \frac{T^2}{M_{Pl}}, \tag{2.21}$$

where g_* is the effective number of relativistic degrees of freedom and $M_{Pl} \simeq 1.22 \times 10^{19}$ GeV is the Planck mass. With the varied choice of parameters, i.e., M_2, M_{DM} and most crucially value of the lightest active neutrino mass, $m_l = 10^{-13}$ eV compels the 3RHN scenario to fall in the strong washout regime similar to 2RHN case or type-I leptogenesis[68]. In the 2RHN case, only two active neutrinos are massive and the distinction between normal hierarchy(NH) and inverted hierarchy(IH) is made. However, for 3RHN the masses of the

heaviest and the lightest active neutrino is almost same which results in the disappearence of the distinction between NH and IH. Also, the 2RHN always falls in the strong washout regime as the decay parameter (K_2) has values greater than 10^3 for larger parameter space. The N_2 decay rate incorporating the Yukawa coupling is given by,

$$\Gamma_2 = \frac{M_2}{8\pi}(Y^\dagger Y)_{22}\left[1-\left(\frac{m_{DM}}{M_2}\right)^2\right]^2 = \frac{M_2}{8\pi}(Y^\dagger Y)_{22}(1-\eta_2)^2. \tag{2.22}$$

The CP asymmetry parameter ε_2 for the decays $N_2 \to l\eta, \bar{l}\eta^*$ is given by,

$$\varepsilon_2 = \frac{1}{8\pi(Y^\dagger Y)_{22}}\sum_{j\neq 2} Im[(Y^\dagger Y)^2]_{2j}\left[f(r_{j2},\eta_2) - \frac{\sqrt{r_{j2}}}{r_{j2}-1}(1-\eta_2)^2\right], \tag{2.23}$$

where, the term $f(r_{j2},\eta_2)$ is expressed as,

$$f(r_{j2},\eta_2) = \sqrt{r_{j2}}\left[1+\frac{(1-2\eta_2+r_{j2})}{(1-\eta_2)^2} ln(\frac{r_{j2}-\eta_2^2}{1-2\eta_2+r_{j2}})\right], \tag{2.24}$$

with $r_{j2} = \left(\frac{M_j}{M_2}\right)^2$, $\eta_2 \equiv \left(\frac{m_{DM}}{M_2}\right)^2$. The frequently appearing $Y^\dagger Y$ in the above equations can be expressed using the CI-parametrization[213],

$$(Y^\dagger Y)_{ij} = \sqrt{\Lambda_i \Lambda_j}(R M_\nu^{diag} R^\dagger)_{ij}. \tag{2.25}$$

An exciting piece of information regarding the $Y^\dagger Y$ is that it is independent of the PMNS matrix. This ensures that the CP-violating phases applicable for leptogenesis is independent of the CP-violating phases in PMNS matrix. In our work, we obtain the yukawa coupling matrix in the range $10^{-6} - 1$. Again, starting with the initial thermal abundance of N_2, wherein its rate of interaction is above the Hubble rate, we solve the Boltzmann equations. It is only feasible if the Yukawa couplings corresponding to N_2 are not very small. In our work, we calculate the Yukawa coupling, which falls in the range applicable to generate the observed baryon asymmetry.

The Boltzmann equations for the number densities of N_2 and N_{B-L}, given by[86],

$$\frac{dn_{N_2}}{dz} = -D_2(n_{N_2} - n_{N_2}^{eq}), \tag{2.26}$$

$$\frac{dn_{B-L}}{dz} = -\varepsilon_2 D_2(n_{N_2} - n_{N_2}^{eq}) - W_2 n_{B-L}, \tag{2.27}$$

respectively. The equilibrium number density of N_2 is given by $n_{N_2}^{eq} = \frac{z^2}{2}K_2(z)$, where $K_i(z)$ is the modified Bessel function of i^{th} type and

$$D_2 \equiv \frac{\Gamma_2}{Hz} = K_{N_2} z \frac{K_1(z)}{K_2(z)} \tag{2.28}$$

is the measure of the total decay rate with respect to the Hubble rate, and W_2 is the total washout rate given by $W_2 = \frac{\Gamma_W}{Hz}$. The total washout term W_2 is the sum of the washout due to inverse decays $l\eta, \bar{l}\eta^* \to N_1$ and the washout due to the $\Delta L = 2$ scatterings $l\eta \leftrightarrow \bar{l}\eta^*, ll \leftrightarrow \eta^*\eta^*$, i.e. $W_2 = W_{2D} + W_{\Delta L=2}$[68], where $W_{2D} = \frac{1}{4}K_{N_2} z^3 K_1(z)$ and,

$$W_{\Delta L=2} \simeq \frac{18\sqrt{10}M_{Pl}}{\pi^4 g_l \sqrt{g_*} z^2 v^4} (\frac{2\pi^2}{\lambda_5})^2 M_2 \bar{m_\varsigma}^2. \tag{2.29}$$

In eq.(2.29), g_l stands for the internal degrees of freedom for the SM leptons, and $\bar{m_\varsigma}$ is the effective neutrino mass parameter, defined by:

$$\bar{m_\varsigma}^2 \simeq 4\varsigma_1^2 m_1^2 + \varsigma_2 m^{2_2} + \varsigma_3^2 m_3^2, \tag{2.30}$$

with $m_i's$ being the light neutrino mass eigenvalues and ς_k is as defined as:

$$\varsigma_k = \left(\frac{M_k^2}{8(m_{\eta_R^0}^2 - m_{\eta_I^0}^2)} [L_k(m_{\eta_R^0}^2) - L_k(m_{\eta_I^0}^2)] \right)^{-1}. \tag{2.31}$$

We assess the final B-L asymmetry n_{B-L}^f just before sphaleron freeze-out by numerically solving the eqs.(2.26) and (2.27), which is further converted into the baryon-to-photon ratio

as,

$$n_B = \frac{3}{4}\frac{g_*^0}{g_*} a_{sph} n_{B-L}^f \simeq 9.2 \times 10^{-3} n_{B-L}^f, \tag{2.32}$$

where $a_{sph} = \frac{8}{23}$ is the sphaleron conversion factor with the consideration of two Higgs doublet. $g_* = 110.75$ is the effective relativistic degrees of freedom at the time of final lepton asymmetry production, and $g_*^0 = \frac{43}{11}$ is the effective degrees of freedom at the recombination epoch. In this work, we have studied the effects on leptogenesis by the variation of parameters such as quartic coupling in the range $10^{-5} - 5$, the probable DM candidate mass in the intermediate-mass regime, i.e., $M_W < M_{DM} \leq 550$ GeV. From this choice of parameters, along with the mass of the lightest neutrino mass in the range 10^{-13} eV for both NH and IH, we calculate the Yukawa couplings for which we achieve n_B^{obs} inferred from the Planck limit 2018, i.e., $(6.04 \pm 0.08) \times 10^{-10}$ at 68% C.L.[210]. Therefore, we get baryogenesis keeping intact the light neutrino mass satisfying the neutrino oscillation data.

2.4.2 Neutrinoless double beta decay

With the light neutrino parameters considered in our work, we can make connections with observable in the on-going experiments. A well known and significant experimental technique of detecting neutrino mass is the neutrinoless double beta decay ($0\nu\beta\beta$)[223–225], with experiments such as KamLAND-Zen, GERDA, KATRIN. In such experiments, what measured is the effective neutrino mass $|m_{\beta\beta}|$ which can be determined by the formula,

$$|m_{\beta\beta}| = \sum_{k=1}^{3} m_k U_{ek}^2 \tag{2.33}$$

where, U_{ek}^2 are the elements of the PMNS matrix with k holding up the generation index. This eq.(2.33) can be further expressed as,

$$|m_{\beta\beta}| = |c_{12}^2 c_{13}^2 m_1 + s_{12}^2 c_{13}^2 m_2 e^{2i\alpha} + s_{13}^2 m_3 e^{2i\beta}| \tag{2.34}$$

where, c_{ij}= $\cos\theta_{ij}$ and s_{ij}= $\sin\theta_{ij}$. It is important to check the satisfying bound of the effective mass with the lightest neutrino mass so that we can relate the current light neutrino parameters giving correct hints to ongoing experiments and their future sensitivity.

2.4.3 Dark matter

The dark matter, which was in chemical and thermal equilibrium in the early Universe, loses its equilibrium state when the pair annihilation rate becomes less than the expansion rate of the Universe, eventually leading the particles to decouple from the cosmic plasma. The relic densities of such thermally produced dark matter candidates can be calculated by solving the Boltzmann equation[226, 92]:

$$\dot{n}_{DM} + 3Hn_{DM} = - < \sigma v > (n_{DM}^2 - (n_{DM}^{eq})^2), \tag{2.35}$$

where, n_{DM} is the number density of the dark matter candidate and n_{DM}^{eq} is the number density of the dark matter candidate in thermal equilibrium. The numerical solution of the Boltzmann equation in terms of partial wave expansion, $< \sigma v >= a + bv^2$ is of the form,

$$\Omega h^2 \approx \frac{1.04 \times 10^9 x_f}{M_{Pl}\sqrt{g_*}(a + 3b/x_f)}, \tag{2.36}$$

where, $x_f = \frac{m_{DM}}{T_f}$, T_f is the freeze-out temperature, also $v^2 \simeq \frac{6}{x_f}$, m_{DM} is the mass of dark matter, g_* is the number of relativistic degrees of freedom at the time of freeze-out, and $M_{Pl} \approx 1.22 \times 10^{19}$ GeV is the Planck mass. Furthermore, we can also express this above expression in a simpler analytical form for the approximation of DM relic abundance as[227],

$$\Omega h^2 \approx \frac{3 \times 10^{-27} cm^3 s^{-1}}{< \sigma v >} \tag{2.37}$$

The corresponding thermal averaged annihilation cross section is therefore given by[228];

$$< \sigma v >= \frac{1}{8m_{DM}^4 T K_2^2(m_{DM}/T)} \int_{4m_{DM}^2}^{\infty} \sigma(s - 4m_{DM}^2)\sqrt{s} K_1(\sqrt{s}/T) ds, \tag{2.38}$$

where, K_1 and K_2 are the modified Bessel functions, m_{DM} is the mass of dark matter candidate and T is the temperature. In our model, we have considered one of the neutral component of the scalar doublet η , i.e, η^0 to be the dark matter candidate which resembles that with the inert doublet model discussed in the papers[33, 199, 200, 73, 72, 201–205, 34, 206, 75, 207, 36]. From the literature[229], we can express the effective cross-section as,

$$\sigma_{eff} = \sum_{i,j}^{N} < \sigma_{ij} v > \frac{g_i g_j}{g_{eff}^2} (1+\Delta_i)^{3/2} (1+\Delta_j)^{3/2} e^{(-x_f(\Delta_i+\Delta_j))}, \tag{2.39}$$

with, $\Delta_i = \frac{m_i - m_{DM}}{m_{DM}}$ and $g_{eff} = \sum_{i=1}^{N} g_i (1+\Delta_i)^{3/2} e^{-x_f \Delta_i}$.

In the above equation, m_i denotes the mass of the heavier inert Higgs doublet. Therefore, the expression for the thermally averaged cross section is given by

$$< \sigma_{ij} v >= \frac{x_f}{8 m_i^2 m_j^2 m_{DM} K_2(\frac{m_i x_f}{m_{DM}}) K_2(\frac{m_j x_f}{m_{DM}})} \times \int_{(m_i+m_j)^2}^{\infty} \sigma_{ij}(s - 2(m_i^2 + m_j^2)) \sqrt{s} K_1(\frac{\sqrt{s} x_f}{m_{DM}}) ds. \tag{2.40}$$

The only parameters mainly affecting the relic is the DM-Higgs coupling (λ_L) and the mass differences between the inert scalars. By appropriate choice of λ_L and mass splitting, it is possible to generate the correct relic abundance for DM mass around 500GeV. However, it is impossible to get the observed relic density below 500 GeV of dark matter mass, if the dark matter is produced thermally. Hence, we approach the non-thermal production of dark matter production mechanisms and study its consequences within the IHDM desert.

A non-thermal contribution in the production of relic abundance can be useful in generating the correct relic for masses of dark matter within the IHDM desert. The addition of the non-thermal part can enhance the under-abundant relic, which was observed in the IHDM desert to satisfy the Planck limit. This can be actually achieved by the late decay of the heavy particle, in our case N_1 decays to DM and SM leptons, i.e. $N_1 \to l\eta, \bar{l}\eta^*$, resulting in the production of a correct relic of the DM candidate(η_R^0). We proceed with the method as discussed in[230], and solve the coupled Boltzman equations shown below to calculate the

number densities of DM candidate and N_1:

$$\begin{aligned}\frac{dn_{DM}}{dt}+3Hn_{DM} &= -<\sigma v>(n_{DM}^2-(n_{DM}^{eq})^2)+N\Gamma_{N_1}n_{N_1},\\ \frac{dn_{N_1}}{dt}+3Hn_{N_1} &= -\Gamma_{N_1}n_{N_1},\end{aligned} \tag{2.41}$$

where N is the average number of DM particles produced on the decay of N_1, and Γ_{N_1} is the decay width of N_1. We then move towards the analytical solution of the Boltzmann equation for n_{N_1} by taking into consideration some of the crucial assumptions, that the co-moving entropy density(g_{*s}) and co-moving energy density(g_*) is almost constant. We now transform the above equation interms of Y_{DM} and Y_{N_1} by using the relation $Y_{DM}=\frac{n_{DM}}{s}$ and $Y_{N_1}=\frac{n_{N_1}}{s}$ where $s=\frac{2\pi^2 g_{*s}T^3}{45}$ is the entropy density. The final equation we obtain on changing the variable t to $x=\frac{M_{DM}}{T}$ and also inserting the above variables:

$$\frac{dY_{DM}}{dx}=-\frac{<\sigma v>s}{Hx}(Y_{DM}^2-(Y_{DM}^{eq})^2)+NrxY_{N_1}(x_0)exp(-\frac{r}{2}(x^2-x_0^2)). \tag{2.42}$$

In eq.(2.42), $r=\frac{\Gamma_{N_1}}{Hx^2}=\left(\frac{\Gamma_{N_1}M_{Pl}}{\pi M_{DM}^2}\right)\sqrt{\frac{90}{g_*}}$ is a constant depending upon the deacy width of the heavy decaying particle and $Y_{N_1}(x_0)$ is the initial abundance of N_1. After finding the numerical solution of eq.(2.42), we obtain the present day abundance of DM and further we implement this solution in calculating the relic abundance of DM in the present Universe using the equation:

$$\Omega h^2=\frac{M_{DM}Y_0 s_0}{\rho_c}, \tag{2.43}$$

where, $\rho_c\sim 1.05\times 10^{-5}h^2$ GeVcm^{-3} is the critical density of the Universe, $s_0\sim 2891.2\,cm^{-3}$ is the current entropy density and $h=0.72$ is the Hubble parameter.

As we know, the decay of N_1 release entropy which may mimic the abundance light element that are involved in the big-bang nucleosynthesis (BBN). Hence, the decay of N_1 must not occur during or after the epoch of the BBN[34]. Thus, we get a constraint on the minimum value of decay width of N_1, i.e., $\Gamma_{N_1}\geq\Gamma_{N_1,min}\equiv 6.58\times 10^{-25}$ GeV, arising from the consideration that the decay lifetime of N_1 should be less than 1 second. Again, an upper

bound on the decay width, i.e. $\Gamma_{N_1} \leq \Gamma_{N_1,max} \equiv \frac{M_{DM}^2}{x_0} \times 10^{-18}$ GeV is a manifestation of the fact that the decay of N_1 should take part mostly after the DM candidate freezes out thermally so as to give adequate contribution towards the relic abundance. Thus, we investigate the limitations that we encountered during the thermal production of the relic and see for what benchmark values of the free parameters Γ_{N_1} and $Y_{N_1}(x_0)$ we can have correct relic abundance within the IHDM desert even for high mass splitting.

As we have considered the lightest stable scalar particle to be a probable dark matter candidate, thus, the spin independent scattering cross section of the SM Higgs is expressed by[72]:

$$\sigma_{SI} = \frac{\lambda_L^2 f^2 m_\mu^2 m_n^2}{4\pi m_h^4 M_{DM}^2} \tag{2.44}$$

where, $\lambda_L = (\lambda_3 + \lambda_4 + \lambda_5)/2$ is the quartic coupling taking part in the DM-Higgs interaction, $m_\mu^2 = m_n M_{DM}/m_n + M_{DM}$ is the DM-nucleon reduced mass and f is the Higgs-nucleon coupling which is estimated to be $f = 0.32$[231]. There also can be a Higgs portal coupling independent DM-nucleon scattering cross-section at a one-loop level[232]. However, by appropriate choice of the mass splitting between the scalar components, we can generate spin-independent scattering cross-section much lower than that obtained from direct detection experiment XENON1T.

2.5 Numerical analysis and results

In this study, we choose the dark matter mass in the intermediate-mass range, $M_W < M_{DM} \leq 550$ GeV, and study the consequences of neutrino mass, neutrinoless double beta decay and baryon asymmetry of the Universe. The plot in the first row of fig.(2.2) depicts that the observed baryogenesis is satisfied for almost the entire IHDM desert for NH, whereas, in case of IH, baryogenesis is obtained for dark mass above 300 GeV with very scanty points. Furthermore, for N_2 leptogenesis in the scotogenic model, we can conclude the mass of the next to the lightest RHN must be greater than 10^7 GeV, which has risen up the TeV scale

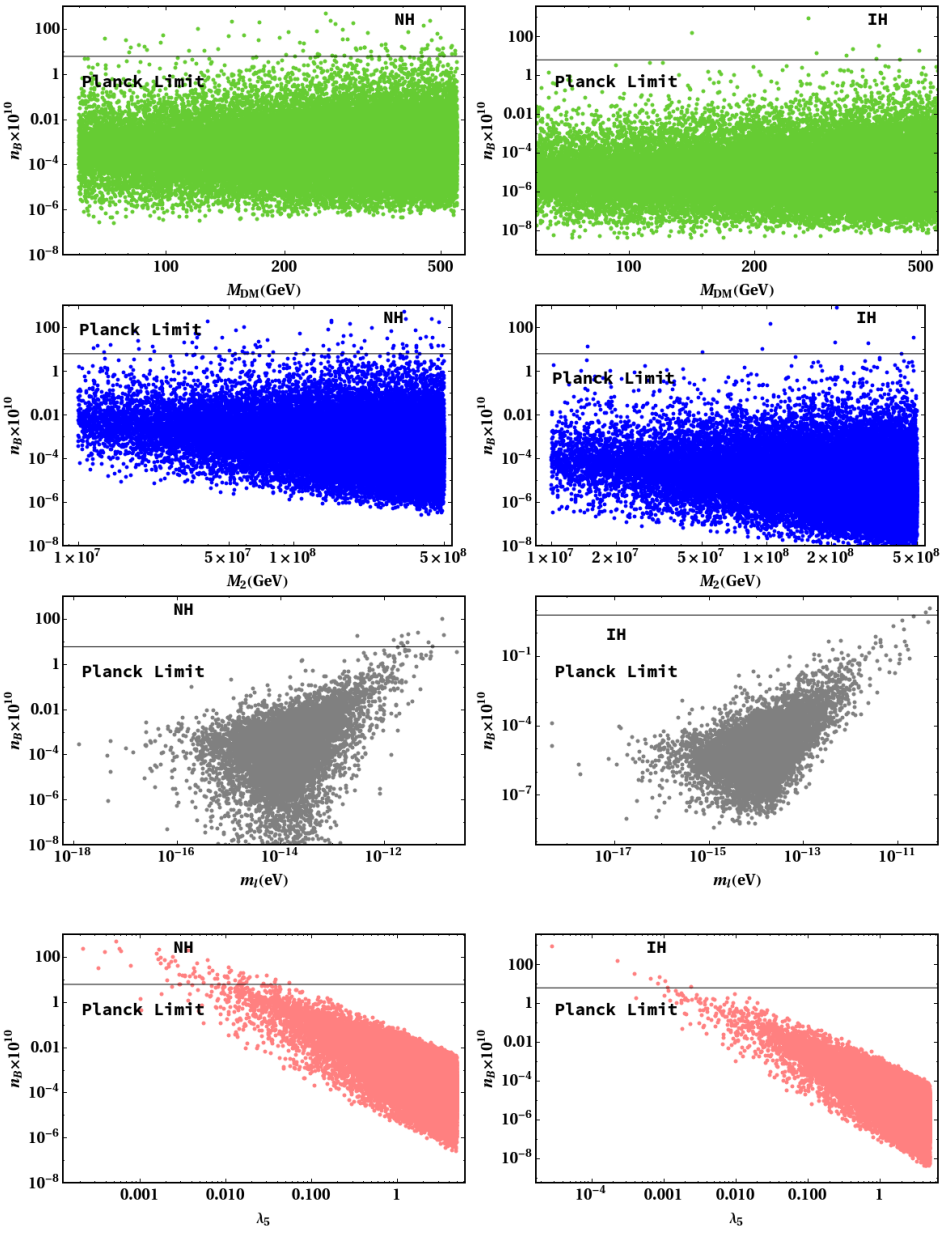

Fig. 2.2 Plots in the first-row show baryon asymmetry as a function of dark matter mass (M_{DM}), the second-row show baryon asymmetry as a function of right-handed neutrino mass (M_2), in third-row baryon asymmetry as a function of the lightest neutrino mass eigenvalue is shown. The fourth row depicts baryon asymmetry as a function of the absolute value of quartic coupling ($|\lambda_5|$) for NH and IH, respectively. The black horizontal line gives the current Planck limit for BAU.

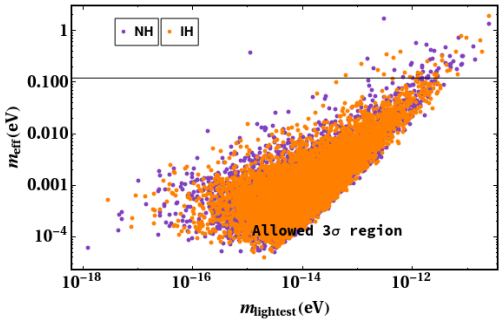

Fig. 2.3 Effective mass as a function of lightest neutrino mass eigenvalue for NH/IH. The horizontal(black) line is the upper limit for the effective mass ($m_{\beta\beta}(eV) \sim 0.12(eV)$) of light neutrinos obtained from KamLAND-Zen experiment and the red vertical line depicts the upper bound given by the Planck limit for the summation of light neutrino masses.

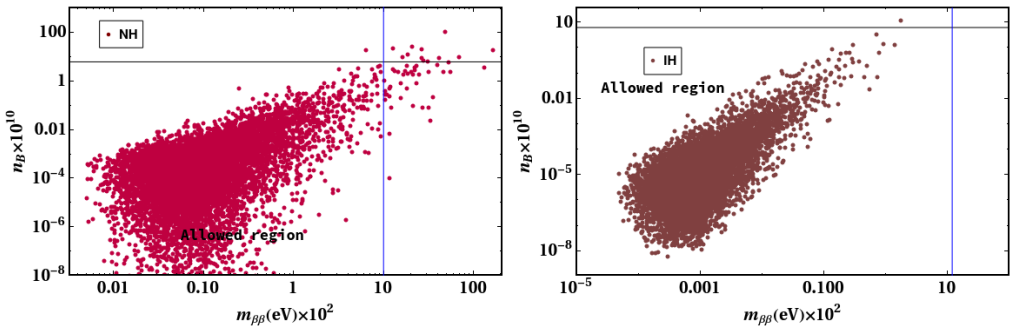

Fig. 2.4 Baryon asymmetry as a function of effective mass of neutrino for NH/IH. The horizontal(black) line is the Planck limit for BAU and the vertical(blue) line depicts the KamLAND-Zen limit for $0\nu\beta\beta$.

thereby enhancing the washout effect. Hence, in our work, we have chosen the RHN masses M_1, M_2 and M_3 in the range $10^4 - 5\times10^5$ GeV, $10^7 - 5\times10^8$ GeV and $10^{12} - 5\times10^{13}$ GeV respectively.

The first row of fig.(2.2) shows the variation between the baryon asymmetry of the Universe and the dark matter mass (M_{DM}). In the second row we have the variation of BAU results with the mass of the next to lightest RHN M_2 for both NH and IH and thus obtain the parameter space of M_{DM} and M_2 that satisfies the currently observed value of BAU in both the mass orderings. From the results of M_2 vs. η_B, we see that the entire range chosen for N_2 generates BAU, whereas in the case of IH, very few points above 5×10^7 GeV satisfies the

Planck limit for BAU. We calculate the mass eigenvalues of light neutrinos for the scotogenic

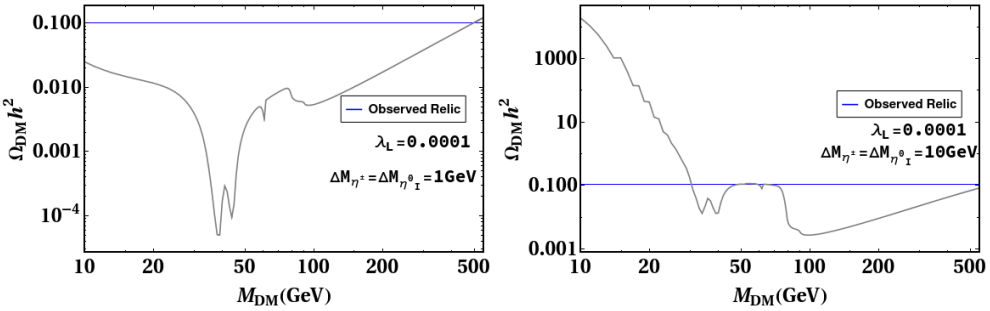

Fig. 2.5 Variation of relic abundance of DM in the intermediate dark matter mass range. Planck limit for the observed relic abundance is given by the horizontal(blue) line. The V shaped portion at around $M_{DM} \approx M_h/2$ is the resonance in the annihilation of DM into SM fermions mediated via Higgs boson(h) in the s-channel.

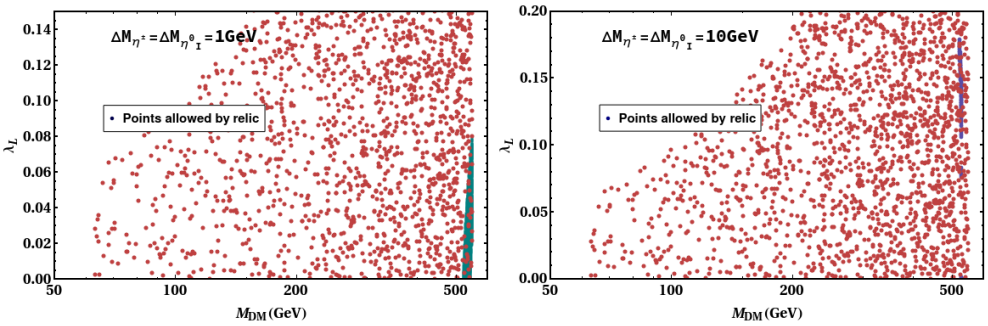

Fig. 2.6 The allowed region of parameter space in λ_L-M_{DM} plane from the requirement of satisfying the relic abundance and depiction of the strict constraints from dark matter direct detection experiment,XENON1T. The red points corresponds to the region allowed by direct detection experiment and the small vertical lines in both the panels of the figure are the points that generate the observed relic abundance.

model by keeping some variables(M_k,λ_5,η^0_R and η^0_I) fixed as mentioned earlier and solving the model parameters. A plot of baryogenesis vs. the lightest neutrino mass eigenvalue, m_l is shown in the third row of fig.(2.2), where the left panel shows the variation for NH and the right panel for IH. Scanning the whole parameter space, we can clearly see that for NH, there are few points in the range $m_l = 10^{-13} - 10^{-12}$ eV, satisfying the Planck limit for observed baryogenesis. However for IH, the points satisfying baryogenesis becomes very scarce. Thus,

we can conclude that the NH is more preferable in terms of BAU than IH in our study. The entire work is carried out for quartic coupling $|\lambda_5| = 10^{-5} - 5$. Therefore, we analyze the parameter space of the quartic coupling satisfying the observed baryon asymmetry, which can be estimated to be $\mathcal{O}(10^{-2} - 5)$ as shown in the last row of fig. (2.2) for NH. But the same analysis differ incase of IH, wherein very few points below $|\lambda_5| = 10^{-2}$ satisfies BAU. Thus, the parameter space taken in our study is more inclined towards generating BAU for NH compared to IH. As we have also studied $0\nu\beta\beta$ in this work and the variation of $m_{\beta\beta}$ vs. m_l for NH and IH are shown in fig.(2.3). Here, the horizontal line is the upper limit for the effective mass of active neutrinos obtained from KamLAND-Zen experiment. Thus, we can see that our study satisfies this constraint as maximum of the points for both NH and IH lie below the upper limit. Moreover, a correlative analysis of the points satisfying both effective mass and baryogenesis is also shown in fig.(2.4). This draws an interesting result as we have seen points satisfying both BAU and $0\nu\beta\beta$ in NH. Whereas for IH, we merely have same points obeying BAU and $0\nu\beta\beta$ simultaneously.

The probable candidate of DM will be the lightest particle among the inert Higgs doublet. In our study, η_R^0 is considered to be a source of DM, with the assumption of it being the lightest of all scalars. Therefore, it's relic abundance is calculated by implementing first this minimal scotogenic model in `Feynrules`[233] and then using the computational package `MicrOmega 5.0.4`[234]. The relic abundance as a function of the DM mass M_{DM} is manifested in fig.(2.5), where, the DM-Higgs coupling is taken to be as low as $\lambda_L = 0.0001$ and the mass differences $\Delta M_{\eta^\pm} = \Delta M_{\eta_I^0} = 1$ GeV (left panel). Also, in fig.(2.5), we have shown a similar plot of relic *vs.* M_{DM} for higher values of $\Delta M_{\eta^\pm} = \Delta M_{\eta_I^0} = 10$ GeV (right panel). From fig.(2.5), we can anticipate that for low mass splitting between the scalars , i.e., $\Delta M_{\eta^\pm} = \Delta M_{\eta_I^0} = 1$ GeV, the relic is suppressed in the low mass regime due to the increase in co-annihilation between the different components of inert scalar doublet. Whereas, in the high mass regime for $\Delta M_{\eta^\pm} = \Delta M_{\eta_I^0} = 10$ GeV the relic is suppressed relic because

the annihilation contribution of the electroweak bosons increases with the mass square differences among the inert scalars.

Furthermore, instead of fixing the DM-Higgs coupling, we show the allowed region of parameter space in the $\lambda_L - M_{DM}$ plane from the obligation of satisfying the correct relic abundance depicted in fig.(2.6). With the relic abundance bound on the $\lambda_L - M_{DM}$ plane, there also exist strict constraint from the dark matter direct detection experiment XENON1T. The scattered points in fig.(2.6) corresponds to the values of M_{DM} and λ_L, which are allowed from the direct detection bound of XENON1T and the small dark portion refer to the points allowed by the current value of relic density. Thus, we can see that there exists a coincidence of both points signifying the parameter space, which obeys constraints from both the cosmological aspects mentioned above. We see a significant difference in the parameter space of λ_L *w.r.t*. the mass difference of the scalars. Hence, we can confirm the choice of mass difference is of utmost importance in determining the relic abundance of dark matter when we donot introduce the non-thermal production of DM[232].

Dark matter relic density primarily depends on the dark matter mass, Higgs portal coupling, and mass differences with the LSP and nLSP[1]. In the low mass region for $M_{DM} < 10$ GeV, most dominating DM annihilation processes are to the SM fermions only, and due to small coupling strength and mass, we get an overabundance of the relic density. Moreover, the dominant part of the points ruled out by the Higgs/Z invisible decay width and direct detection constraints for the low mass. Within IHDM, irrespective of the choice of parameter spaces, the region in between $M_W < M_{DM} \leq 530$ GeV does not give observed relic abundance value due to the very high annihilation rate of $DM + DM \to W^{\pm}W^{\pm}, ZZ$[204, 235, 236]. However, by considering different production mechanisms as discussed by[34, 230], we can work out the on the IHDM desert region to get observed relic abundance. Here we consider the decay of a particle N_1, which produces dark matter non-thermally, and by adjusting suitable decay width and initial abundance of dark matter candidate, we can generate observed relic density

[1]Lightest stable particle and next to lightest stable particle.

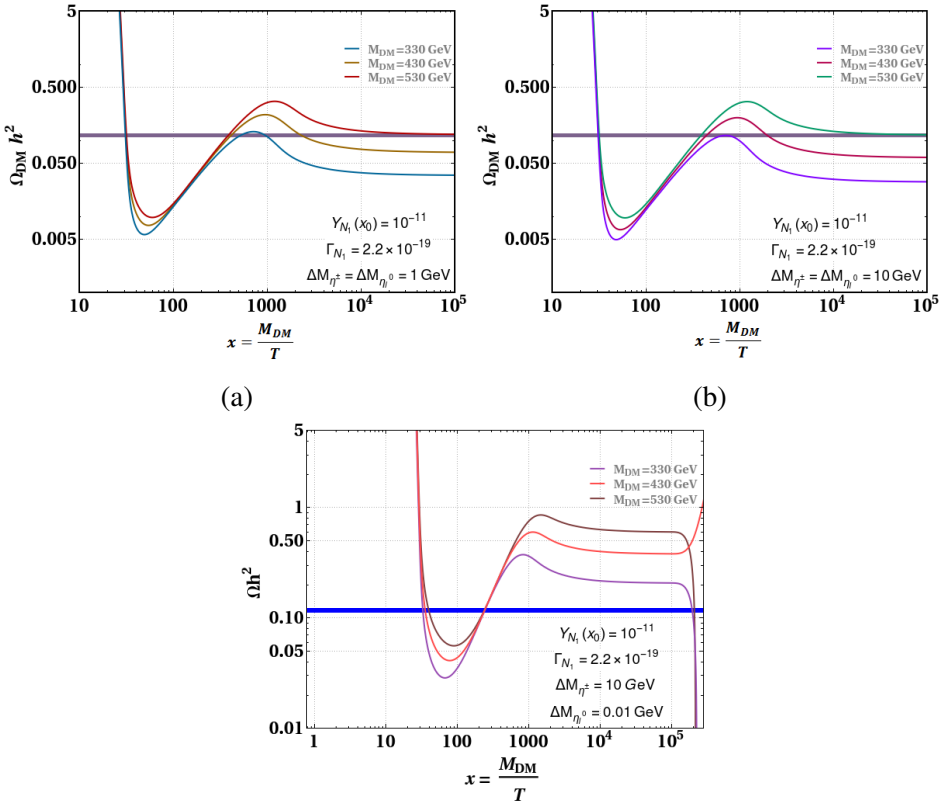

Fig. 2.7 Variation of relic abundance vs $x(= M_{DM}/T)$ for three different values of dark matter masses with fixed values of Γ_{N_1} and $Y_{N_1}(x_0)$ as given in the plot. The corresponding parameters which contribute in determining relic are kept fixed with values: (a) $\Delta M_{\eta^\pm} = \Delta M_{\eta_I^0} = 1$ GeV, (b) $\Delta M_{\eta^\pm} = \Delta M_{\eta_I^0} = 10$ GeV, and (c) $\Delta M_{\eta^\pm} = 10$ GeV and $\Delta M_{\eta_I^0} = 0.01$ GeV, $\lambda_L = 0.0001$, $\lambda_2 = 0.2$ and $M_h = 125.5$ GeV.

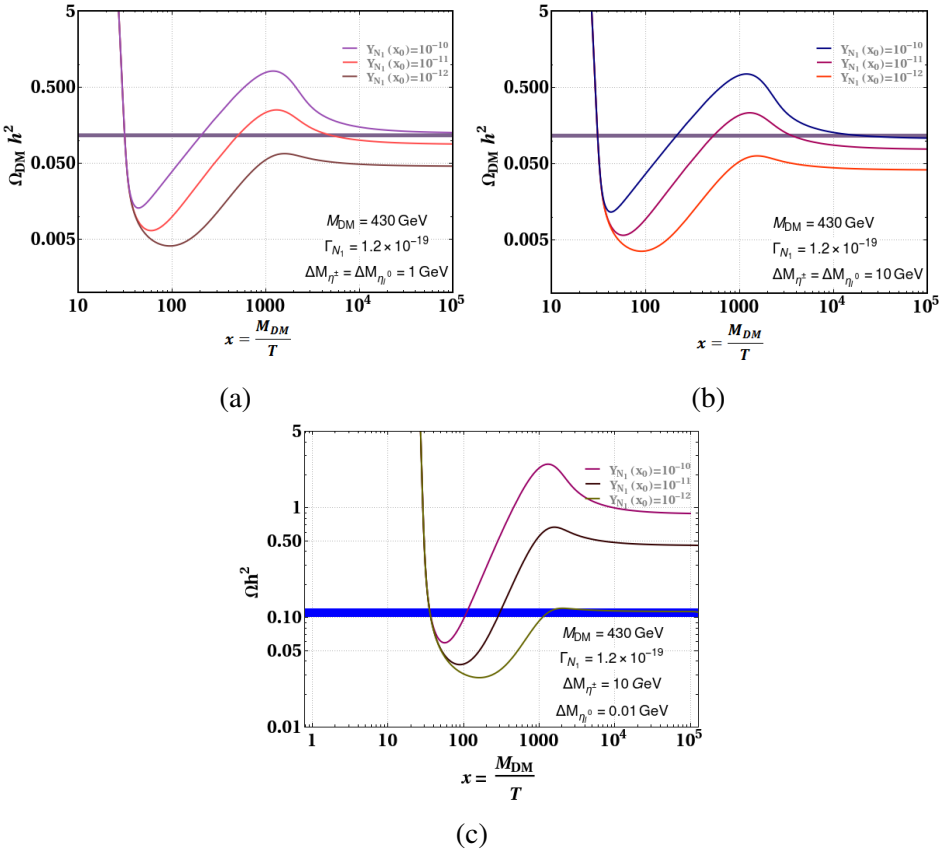

Fig. 2.8 Plot of relic abundance vs $x(= M_{DM}/T)$ with DM mass fixed at $M_{DM} = 430$ GeV and $\Gamma_{N_1} = 1.2 \times 10^{-19}$ for three different values of $Y_{N_1}(x_0)$. The corresponding parameters which contribute in determining relic are kept fixed with values: (a) $\Delta M_{\eta^\pm} = \Delta M_{\eta_I^0} = 1$ GeV, (b) $\Delta M_{\eta^\pm} = \Delta M_{\eta_I^0} = 10$ GeV and (c) $\Delta M_{\eta^\pm} = 10$ GeV and $\Delta M_{\eta_I^0} = 0.01$ GeV, $\lambda_L = 0.0001$, $\lambda_2 = 0.2$ and $M_h = 125.5$ GeV.

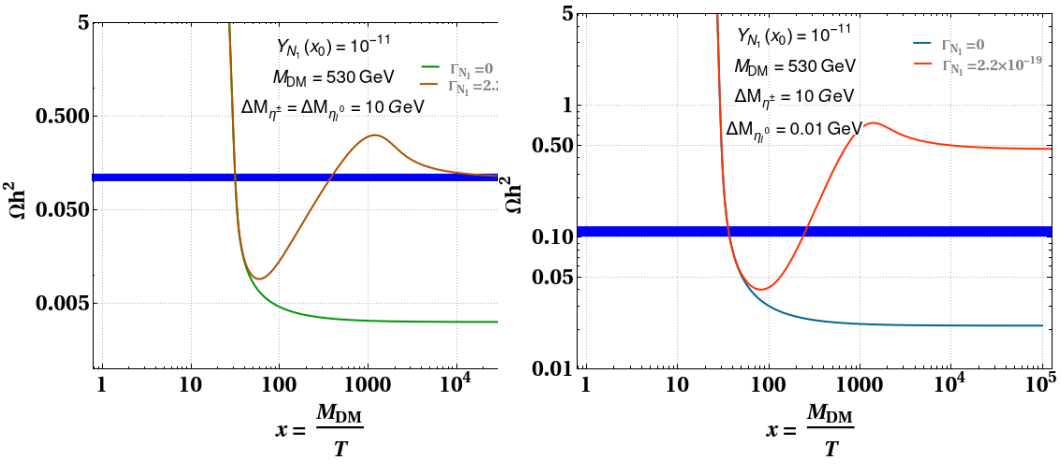

(a) (b)

Fig. 2.9 Relic abundance vs $x(= M_{DM}/T)$ plot with dark matter mass fixed at 530 GeV and $Y_{N_1}(x_0) = 10^{-11}$ for two values of Γ_{N_1}. $\Gamma_{N_1} = 0$ corresponds to thermal production and $\Gamma_{N_1} = 2.2 \times 10^{-19}$ signifies non-thermal production. The corresponding parameters which contribute in determining relic are kept fixed with values: (a) $\Delta M_{\eta^\pm} = \Delta M_{\eta_I^0} = 10$ GeV(left panel), (b) $\Delta M_{\eta^\pm} = 10$ GeV and $\Delta M_{\eta_I^0} = 0.01$ GeV(right panel), $\lambda_L = 0.0001$, $\lambda_2 = 0.2$ and $M_h = 125.5$ GeV.

within the IHDM desert. From fig.(2.5), we can see the deviation in relic abundance, taking into consideration the crucial parameter, i.e., the mass splitting among the scalars of the inert doublet. For $\Delta M_{\eta^\pm} = \Delta M_{\eta_I^0} = 1$ GeV, we get the correct relic abundance corresponding to $M_{DM} = 530$ GeV, whereas for $\Delta M_{\eta^\pm} = \Delta M_{\eta_I^0} = 10$ GeV, we fail to generate the relic. Therefore, we proceed with the non-thermal production of dark matter to see if the desired relic is obtained for the above value of dark matter and masses even lower than it. We consider the low mass splitting case with M_{DM}= 530 GeV and by appropriate choice of the decay width(Γ_{N_1}), we see that for $Y_{N_1}(x_0) = 10^{-11}$ GeV, it produces the correct relic abundance. Again for high mass splitting, the deviation in thermal and non-thermal production of the relic is observed. We verify the result obtained in the right panel of fig.(2.5), again by fig.(2.9), that dark matter is underabundant thermally. It shows that for M_{DM}=530 GeV and the choice of other parameters, $\Gamma_{N_1} = 2.5 \times 10^{-19}$ and $Y_{N_1}(x_0) = 10^{-11}$, we obtain the relic, whereas for $\Gamma_{N_1} = 0$, there is an underabundant production of relic. We also do a relative study for three

benchmark values of dark matter in the low mass splitting as well as the high mass splitting scenario depicted in fig.(2.7). We now fine-tune the decay width in order to obtain the correct relic abundance for $M_{DM} = 430$ GeV, which was underabundant for the values shown in fig.(2.7). Thus, fig.(2.8) showcases the two different mass splitting scenarios for $M_{DM} = 430$ GeV, and investigate the values of Γ_{N_1} and $Y_{N_1}(x_0)$ which satisfies the correct relic abundance. We have also shown the variation of relic abundance for three benchmark values of dark matter in consideration with different values of scalar mass splittings, i.e $\Delta M_{\eta^\pm} = 10$ GeV and $\Delta M_{\eta_I^0} = 0.01$ GeV in the fig. (2.7c). We see a deviation in the curves which were previously satisfying observed relic when similar mass splittings between the scalars were considered. However, for $M_{DM} = 430$ GeV, $\Gamma_{N_1} = 1.2 \times 10^{-19}$ and $Y_{N_1}(x_0) = 10^{-12}$ it is possible to generate the correct relic abundance inspite of the inequality between the values of scalar mass splittings. This can be seen in the fig. (2.8c). Also in the right panel of fig.(2.9), due to different values of scalar mass splittings as mentioned earlier, we see a vast deviation in the curves satisfying the relic abundance. Therefore, we can see a distinct variation of $\Delta M_{\eta^\pm}$, $\Delta M_{\eta_I^0}$, Γ_{N_1} and $Y_{N_1}(x_0)$ *w.r.t.* dark matter mass resulting in the production of correct relic abundance.

2.6 Summary

In this work, we study an extension of the SM popularly known as the *scotogenic model*, which is extended by a Higgs doublet (η) and three singlet neutral fermions (N_k). An additional Z_2 charge is assigned in the model, and all the SM particles are even under it while additional fields are odd. The possibility of a DM candidate comes from the Z_2 odd lightest particle. We carry out this work with the dark matter mass strictly focusing in the intermediate dark matter mass range, also known as the inert Higgs doublet model (IHDM) desert, which lies between $M_W < M_{DM} \leq 550$ GeV. Along with DM, baryogenesis via the mechanism of thermal leptogenesis and neutrinoless double beta decay is also addressed

in this work. Leptogenesis is a result of the decay of Z_2 odd fermions, *i.e*, the heavy RHN, which occurs via the out-of-equilibrium decay into the SM leptons and the inert Higgs doublet. The out-of-equilibrium decay of $N_2 \to l\eta, \bar{l}\eta^*$, where η is the inert Higgs doublet constituting the dark matter candidate η_R^0 , generates the observed baryon asymmetry of the Universe. The final lepton asymmetry is generated only because of the asymmetry created by the decay of N_2, which is the next to lightest RHN. Again, for two different choice of mass splitting between the DM (LSP) and the next heavier scalar (nLSP), we study the relic abundance of the dark matter candidate (lightest of η). We also study the mixture of thermal and non-thermal production of DM abundance for various masses within the IHDM desert. In our study, the non-thermal DM within the IHDM desert is produced via late decays of N_1. Therefore, the lifetime of N_1 will be more than sphaleron time resulting in the discripency to generate the baryon asymmetry. This is because the decay width of N_1 considered in our work for the non-thermal production of DM is very small. Also we can say that the mass splitting between the inert scalars are crucial for thermal production of DM unlike that for non-thermal prodcution of DM. Although the inequality in the values of scalar mass splittings do create a difference in generating the observed relic abundance via non-thermal production. As our model is compatible with baryogenesis studied in the IHDM desert, we are successfully able to show correlation plot of dark matter mass (M_{DM}), RHN mass (M_2), lightest neutrino mass eigenvalue (m_l) and quartic coupling parameter (λ_5) with the latest observed value of BAU. We consider a particular range of quartic coupling, between $10^{-2} - 5$, which is accountable for reproducing the observed baryon asymmetry of the Universe by the decay of N_2 with a mass in the range $10^7 - 5 \times 10^8$ GeV. We also calculate the light neutrino mass eigenvalues and check its consistency with the experimental bounds obtained from KamLAND-Zen by the neutrinoless double beta decay method. The correlation between the BAU result and $0\nu\beta\beta$ has a very constrained space in our work for both the mass ordering. From the synchronous study of $0\nu\beta\beta$ and baryogenesis, it is evident that both the observable

are loosely correlated in our model. Moreover, the light neutrino mass eigenvalues obtained from this framework are more likely to satisfy the KamLAND-Zen limit for $m_{\beta\beta}$, and at the same time, they obey Planck limit for generating the observed BAU. From the correlation plots between the various parameters and observed Planck limit of BAU, we can conclude that the NH is more preferable over the IH.

The significant conclusion we observe from our analysis is that the mass splitting, $\Delta M_{\eta^\pm} = \Delta M_{\eta_I^0}$ plays a vital role in the production of relic abundance via thermal production only. As, for thermal production of DM, we could generate relic for $\Delta M_{\eta^\pm} = \Delta M_{\eta_I^0} = 1$ GeV but failed in the case of $\Delta M_{\eta^\pm} = \Delta M_{\eta_I^0} = 10$ GeV for the same value of $\lambda_L = 0.0001$, which therefore satisfies the LEP constraints[237] as it rules out values of mass splitting greater than 8 GeV. This draws attention to how effective the mass splitting could be in the IHDM. It also motivates us to study the non-thermal production of dark matter. For non-thermal production of dark matter, we observe current relic abundance for the appropriate choice of decay width and coupling parameters with $\Delta M = 1$ GeV and $\Delta M = 10$ GeV. However, for $\Delta M_{\eta^\pm} = 10$ GeV and $\Delta M_{\eta_I^0} = 0.01$ GeV, we observe certain variations in the relic abundance curve. Thus, realising that the choice of mass splitting doesnot affect the relic abundance generated via non-thermal production unless they are equal.